Algorithms for fast axisymmetric drop shape analysis measurements by a charge coupled device video camera and simulation procedure for test and evaluation

Lorenzo Busoni, Marcello Carlà,[a] and Leonardo Lanzi
Department of Physics, University of Florence and I.N.F.M. (Istituto Nazionale per la Fisica della Materia), Via G. Sansone 1, 50019 Sesto Fiorentino, Firenze, Italy

(Received 11 September 2000; accepted for publication 20 November 2000)

A set of fast algorithms for axisymmetric drop shape analysis measurements is described. Speed has been improved by more than 1 order of magnitude over previously available procedures. Frame analysis is performed and drop characteristics and interfacial tension γ are computed in less than 40 ms on a Pentium III 450 MHz PC, while preserving an overall accuracy in $\Delta\gamma/\gamma$ close to 1×10^{-4}. A new procedure is described to evaluate both the algorithms performance and the contribution of each source of experimental error to the overall measurement accuracy. © *2001 American Institute of Physics.* [DOI: 10.1063/1.1364666]

I. INTRODUCTION

The analysis of the profile of an axisymmetric drop of liquid—either a sessile or a pendant drop—immersed in a second liquid, has always been considered to be the most reliable and accurate method for measuring interfacial tension at the liquid–liquid interphase. During its long history, after the first description in Bashforth and Adams work in 1883,[1] the exploitation of axisymmetric drop shape analysis (ADSA) was severely limited by the lack of the necessary technological facilities as a low distortion image acquisition device and computing power at an affordable price. Current possibility to meet at low price both requirements have induced a renewed interest into the use of ADSA and it is considered to be a routine method for the study of liquid–liquid interface, instead of relegating it to the role of a refined calibration procedure.[2,3] In the course of ADSA history, several mathematical procedures have been proposed to extract the physical quantity of interest, interfacial tension, from the raw experimental data, which consist of a set of point coordinates describing the drop profile. In Refs. 4–12 in Ref. 4 an evolution can be traced from the original ''selected plane method''—in which a very limited amount of experimental points were used—to algorithms that make use of the fit of the whole set of profile points, clearly at the expense of a greater computational burden. See also Refs. 5 and 6 for a discussion on several frequently used algorithms.

Currently the most convenient way to implement an ADSA apparatus is to connect a solid state video camera equipped with a charge coupled device (CCD) or a charge injection device[7] to a personal computer or a workstation through a frame grabber. It is possible by this method to fully automate the measuring procedure. Using fast algorithms, the method is also suitable for kinetic measurements, e.g., it is possible to record the time evolution of interfacial tension in a relaxation process or the dependence of interfacial tension upon another time varying quantity, as in the compression–expansion cycles of a film supported by a variable size drop.[8] To this purpose we have implemented fast algorithms optimized for the use of a CCD video camera. Thereafter, we implemented a new software procedure that simulates most sources of experimental errors intrinsic to the measuring technique. Then we tested every algorithm for both speed and accuracy under several different sources of error. The test procedure simulates the whole process of drop image formation and digitization in a CCD video camera and applies errors and disturbances in a controlled manner. Then, the resulting pseudoexperimental frame is analyzed by the algorithm under test and performance is registered in recovering the correct drop parameters despite added disturbances.

Both the ADSA algorithms and the test procedure have been initially implemented as a set of Fortran routines for the DEC (formerly Digital Equipment Corporation, Maynard, MA) F77 compiler and the VMS operating system.[9] After moving to the Unix environment, the C language has been used to rewrite some routines and to write new ones, when convenient.

Currently the package is used with the Linux operating system, distribution Red Hat 6.1 or 6.2 (Red Hat Inc., Durham, N.C.) on a 450 MHz Pentium computer.[10]

II. THEORY

The ADSA technique to measure interfacial tension γ consists in the detection of the profile of a sessile (or pendant) drop by use of a video camera or other suitable instrumentation. The drop shape is a function of γ and other parameters, easy to be measured, as it follows from the Young–Laplace equation:

$$\gamma\left(\frac{1}{R_1}+\frac{1}{R_2}\right)=C+gZ(D_1-D_2), \tag{1}$$

where R_1 and R_2 are the radii of the surface at point P of height Z, C is the pressure difference across the interphase in $Z=0$, g the gravity acceleration, and D_1 and D_2, respec-

[a]Author to whom correspondence should be addressed; electronic mail: carla@fi.infn.it

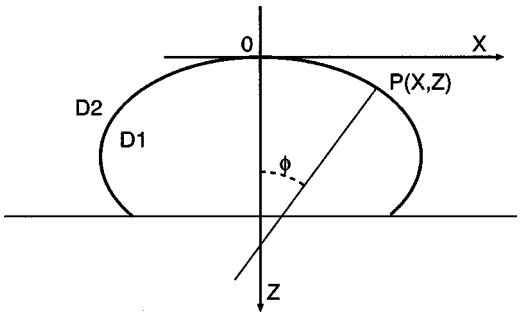

FIG. 1. The shape of an axisymmetric sessile drop. D_1 and D_2 are the densities of the drop liquid and of the surrounding liquid, respectively.

tively, the density of the drop and of the surrounding fluid. For an axisymmetric system—see Fig. 1—Eq. (1) reduces to the Bashforth and Adams equation

$$\gamma\left(\frac{1}{R}+\frac{\sin\varphi}{X}\right)=\frac{2\gamma}{R_0}+gZ(D_1-D_2), \tag{2}$$

where φ is the angle between the Z axis and the external normal to the profile at point P of coordinates X, Z, and R is the radius of curvature at point P in the meridian plane.

At $Z=0$ the curvature radii are identical and equal to R_0, so the pressure difference C is equal to $2\gamma/R_0$; using reduced coordinates $x=X/R_0$, $z=Z/R_0$, $r=R/R_0$, and the *form factor*

$$\beta=g\cdot(D_1-D_2)\cdot R_0^2/\gamma \tag{3}$$

the differential equation for the drop profile is

$$\frac{1}{r}+\frac{\sin\varphi}{x}=2+\beta z \tag{4}$$

or, alternatively, expressing φ and r as a function of z and its derivatives

$$z''(x)=\left[(2+\beta z)\sqrt{1+z'^2}-\frac{z'}{x}\right](1+z'^2). \tag{5}$$

This equation has no analytical solution except for $\beta=0$ (in this case the solution is a circle), but can be integrated numerically. The measure consists in getting β and R_0 from the experimental profile and, knowing g, D_1, and D_2, calculating γ from Eq. (3).

III. EQUIPMENT

In describing the ADSA algorithms we refer to the experimental setup schematically shown in Fig. 2, as we currently use it. The video camera used for profile detection is an Adimec MX12P-8443 (Advanced Image Systems B.V., Eindhoven, The Netherlands), equipped with a 1024 $\times$1024 pixel CCD sensor with 4096 gray levels and capable of 30 frames/s; pixel size is 7.5 μm$\times$7.5 μm. The camera is connected through an Imaging Technology IC-PCI-AM-DIG frame grabber (Imaging Technology Incorporated, Bedford, MA) to an Intel Pentium III, 450 MHz computer.

The computer has control over all the apparatus, as several experimental parameters are of relevance in order to obtain high accuracy measurements: over the control of cell temperature, electrolytical solution composition, and polarization potential at the mercury interface, which are required to perform thermodynamical measurements,[11] the computer has control of the drop surface, the intensity of the lamp that back illuminates the drop and the horizontal alignment of the vibration damping bench, required to keep the drop axisymmetry as described in detail in Ref. 12.

The computer runs a Red Hat Linux 6.1 operating system. The whole application software has been developed lo-

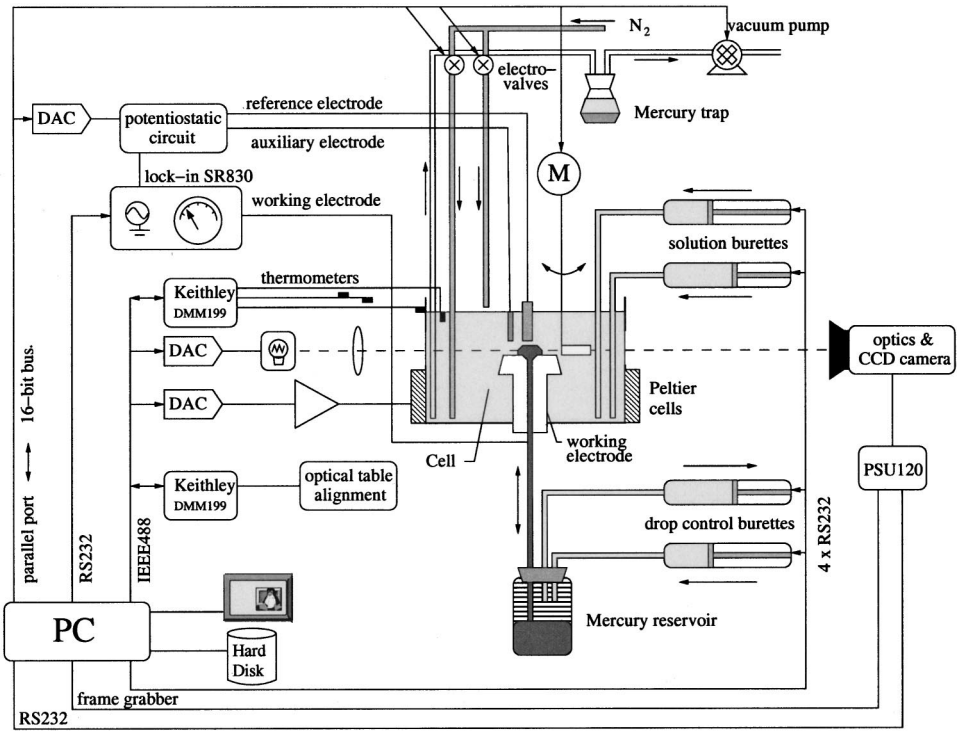

FIG. 2. Block diagram of the apparatus as described in Ref. 8.

cally, except for the frame grabber driver (GOM mbH, Braunschweig, Germany) and the IEEE488 board driver (National Instruments, Austin, TX).

IV. THE MEASURING PROCEDURE

The image of the drop contains a huge amount of useless information: each $1024\times1024\times12$ bit frame, which amounts to 1.5 Mbyte storage size, eventually yields only the two floating point values that we are interested in: R_0 and β. Some other piece of auxiliary information can be extracted from the frame, mainly as a control that the apparatus be working properly, but currently there is no reason (apart from debugging) for storing whole frames during measurements. The first step in processing the frame is extraction of the profile. This reduces the storage requirements to some tens of kbyte, a much more suitable size for storing data for a second step processing.

The second step consists of the fit of the extracted profile with the Bashforth and Adams equation; in past times such computations have had to be deferred to off line processing, until powerful enough computers have been made available at an affordable price. On line processing of the extracted profile, over offering the obvious benefit of making the measurement results immediately available, is currently required in our apparatus for active control of the drop surface, as described in Ref. 8.

All computations in first and second steps are made using the pixel as a convenient unit length; then, a third step is required to scale results according to the geometrical scale factor, to compute β and γ, and apply some minor corrections.

V. PROFILE EXTRACTION

Algorithms normally used for edge detection are probably oversized in this application: it can be safely assumed that a *single* continuous edge *is* actually present in the frame; after a single point has been found along that edge, the profile extraction algorithm can move along the edge in both directions to determine all other experimental points. All pixels not contained in the transition region from dark to light along the edge can be safely ignored. Then the profile extraction can be split into:

(i) finding a point along the edge;
(ii) moving along the edge; and
(iii) determining from the pixel intensity values the coordinates of points along the edge.

The procedure we use for profile extraction is illustrated in Fig. 3. The profile scanning starts at top of the sessile drop (bottom in case of a pendant drop). A string of pixels spanning the full transition region is extracted and the edge position is determined using one of the interpolation algorithms described below. The string is row or column aligned, depending on whether the angle between the Z axis and the external normal to the profile is in the range 45°–135° or out of it. For each row or column a profile point is determined whose coordinates are the row or column index (that coincide with the Z or X coordinates of center of pixels) and the

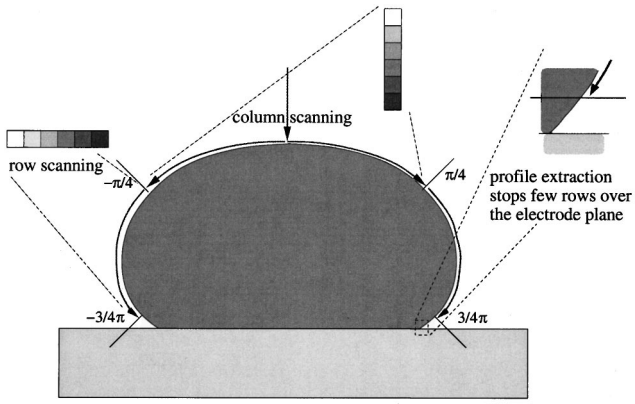

FIG. 3. The profile extraction procedure. Strings of pixel are extracted from the frame, aligned along a row or column, depending upon the profile slope; the edge position is determined by interpolation on the gray levels. The extraction stops a few rows over the electrode plane as accuracy is impaired by overlapping of extracted strings with electrode image.

value given by the interpolation algorithm. The central pixel of next string to be processed is determined by linear extrapolation of the coordinates of the last three to nine points. This step, not strictly required for accuracy, yields the profile slope needed to switch between column scan and row scan and makes the algorithm more robust against the ''loss of the way'' that occasionally may occur.

The interpolation algorithm to calculate the edge position from the illumination intensity values is the most critical part of the profile extraction procedure. Several algorithms have been reviewed in Refs. 13 and 14. Analysis of adjacent linear strings of pixels, that is the use of a rectangular convolution mask $n\times1$, as proposed in Refs. 14, 11, and 15 is considered a better choice over the use of a square convolution mask as the accuracy would receive little benefit from the use of a square mask, at the expense of a consistent increase of computational burden (however, no test has been made in this sense yet). Song[16] located edge position x as the point at which the fraction $\varepsilon(x)=(g(x)-g_2)/(g_1-g_2)$ was equal to a predefined constant ($g(x)$ is the gray level profile and g_1,g_2 correspond to the plateau gray levels at the two sides of the edge). Hansen[17] used a similar algorithm, but while Song determined experimentally that $\varepsilon=0.5$ was the best choice, in agreement with theoretical considerations, Hansen obtained the value 0.67 for best agreement with known values of interfacial tension. Kakiuchi[18] and Pallas[14] instead used the maximum gradient method. Both methods have their justification in the symmetry of the transformations involved in the optical image formation process, as pointed out by Seitz in Ref. 13. In the same article two more methods are quoted: center of mass and Gaussian interpolation of differences of intensity of adjacent pixels. The latter method is based on the observation that the derivative of the intensity profile in the transition region is a function that results from the combination of many unrelated effects. Then, by the central limit theorem this function should be Gaussian. Indeed this conclusion is a justification for the other three methods also, as they require only the symmetry of the intensity function.

Routines have been written to implement the center of

mass method, the halfway method as in Ref. 16, and the maximum gradient method through parabolic interpolation; then, performance of the three methods has been tested both for speed and noise rejection with our simulation procedure, as reported in Sec. IX D. Though all methods have been widely used in past years by several authors, no such comparison had been reported before, especially for the noise rejection evaluation, that results to be one of the most critical parameters.

VI. FIT OF EXPERIMENTAL POINTS AND CALCULUS OF γ

While the shape of a drop depends only upon the adimensional shape factor β, the mapping of experimental points onto the theoretical profile involves several other parameters, namely the scale factor R_0 and the coordinates of the apex (X_0, Z_0). Some authors add one more parameter, i.e., the tilt angle between the drop symmetry axis and the camera vertical axis, to account for instrumentation misalignment. By this way, the least-squares method should be applied minimizing over five parameters.[6] Even if this is, by principle, the most correct procedure, it results rather inconvenient from the point of view of computation time. In case the digitizing device is a CCD video camera and the profile extraction procedure described in Sec. V is used, the number of parameters to be adjusted by the fit routine can be reduced to three without any significant loss of accuracy. In disagreement with Ref. 6, we show in Sec. IX C that tilt angle can be excluded from the minimization procedure as the alignment of the CCD sensor with the local vertical axis can easily be made accurate enough to make negligible the error it introduces. In any case tilt angle, if included in the minimization procedure, cannot account for deviations of the drop supporting orifice from the true horizontal; in this case it is the very condition of axial symmetry of the drop that fails and this effect, which cannot be corrected by a frame rotation, does not seem to have received due attention yet. The second parameter that can be excluded from the minimization procedure is the apex coordinate X_0. The experimental points obtained from the procedure in Sec. V have the property that one of the coordinates is always an integer number not affected by experimental error. Usually a profile is composed of three or five sections: a top section with $|\varphi|<45°$ and integer X coordinates, two lateral sections with $45°<|\varphi|<135°$ and integer Z coordinates and two bottom sections with $|\varphi|>135°$ and integer X coordinates. The average of X coordinates of midpoints of segments whose extremes are the points of identical Z in the two lateral sections yields a first estimate of X_0. These estimate results are accurate enough so that no further refinement is necessary. This has been verified over a wide range of operating conditions (see Secs. IX B and IX D). Then our choice has been to minimize over β, R_0, and Z_0 only. A first estimate for these parameters is obtained by a 4° order polynomial fit on the upper part of the profile, about 1/3 of all data points. The fitted function is $Z=a+bX^2+cX^4$. By comparison with the Taylor expansion of the profile function in $X=0$:

$$Z(X)=Z_0+\frac{1}{2}\frac{d^2Z}{dX^2}\bigg|_0 X^2+\frac{1}{24}\frac{d^4Z}{dX^4}\bigg|_0 X^4+\ldots \tag{6}$$

after substitution of derivatives from Eq. (5), with the boundary conditions $Z'(0)=0$ and $Z(0)=0$, one gets

$$Z''(0)=1$$

and

$$Z'''(0)=\tfrac{3}{4}(4+\beta) \tag{7}$$

and

$$Z_0=a,\quad R_0=\frac{1}{2b},\quad \beta=4\left(\frac{c}{b^3}-1\right). \tag{8}$$

The estimate obtained by this method is not as accurate as can be obtained by the ratio of the equatorial diameter over the equatorial height method,[15] but it has two advantages: it can be used with both sessile and pendant drops and, more important, can be used even when the contact angle is less than 90° and, obviously, the drop has no equator.

The first estimate is then refined by an iterative procedure. Values of X_0, Z_0, R_0, and β are used to calculate an analytical *reference* profile. Differential equation (4) is expanded into the system:

$$\begin{aligned}\frac{d\gamma}{ds}&=2+\beta z-\frac{\sin\varphi}{x},\\ \frac{dx}{ds}&=\cos\varphi,\\ \frac{dz}{ds}&=\sin\varphi,\end{aligned} \tag{9}$$

and integrated by a 4° order Runge–Kutta integration procedure at a constant ds arc step.[19]

A constant $d\varphi$ integration step would reduce system (9) to two equations and would allow the use of tabulated trigonometric functions, speeding up computations, but the algorithm could be used only with sessile drops as in a pendant drop the (X, Z) coordinates are not single-valued functions of φ.

For each experimental point Q_i, the distance d_i from the reference profile is calculated and the expression $e=\Sigma_i d_i^2(\beta,R_0,Z_0)$ is minimized with respect to R_0, Z_0, and β. The minimization of e proceeds by iterative solution of the linearized system[6]

$$\mathbf{H}\Delta\mathbf{p}=\mathbf{E}, \tag{10}$$

where

$$H_{mn}=\sum_i \frac{\partial d_i}{\partial p_m}\cdot\frac{\partial d_i}{\partial p_n},\quad \mathbf{p}=\begin{bmatrix}\beta\\ R_0\\ Z_0\end{bmatrix},\quad E_m=\sum_i \frac{\partial d_i}{\partial p_m}d_i. \tag{11}$$

Once $\Delta\mathbf{p}$ has been determined, a new value $\mathbf{p}'=\mathbf{p}+\Delta\mathbf{p}$ is computed and used to obtain a new reference profile and continue iteration.

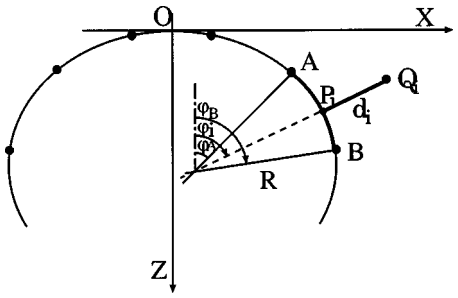

FIG. 4. Calculation of distance d_i from experimental point Q_i to reference profile: coordinates of point P_i on the reference profile are determined by interpolation and used in calculating partial derivatives of d_i.

Distance d_i in Eq. (11) is obtained drawing a circumference through two points in reference profile closest to Q_i, with radius R obtained as

$$R = \frac{\widehat{AB}}{\varphi_B - \varphi_A};$$

then d_i is calculated directly as the distance between Q_i and the circumference by standard analytical geometry formulas, avoiding the iterative procedure used in Ref. 6 that is heavily time consuming. During this computation angle φ_i and coordinates of point P_i are determined (see Fig. 4) and are used to calculate partial derivatives

$$\frac{\partial d_i}{\partial \beta}, \quad \frac{\partial d_i}{\partial R_0}, \quad \frac{\partial d_i}{\partial Z_0}.$$

The first one is tabulated while generating the reference profile: the integration is performed twice, with values of β differing for a small $\delta\beta$; the derivative is calculated as

$$\frac{\partial d}{\partial \beta} = \frac{\Delta \mathbf{P} \cdot \mathbf{n}}{\delta \beta},$$

where $\Delta \mathbf{P}$ is the displacement of point P due to the variation of shape $\delta\beta$, and $\mathbf{n}$ is the versor normal to the profile in P. The actual value of $\partial d_i / \partial \beta$ for each experimental point i is obtained by interpolation.

Other derivatives are calculated as

$$\frac{\partial d_i}{\partial R_0} = \mathbf{P}_i \cdot \mathbf{n},$$

$$\frac{\partial d_i}{\partial Z_0} = -\cos(\varphi_i).$$

The routine that computes distances d_i starts analyzing the points at the apex of the drop and proceeds toward the base; when the distance becomes greater then a threshold value (typically, three pixels) the routine stops. This partial analysis is sufficient to improve the value of the fit parameters β, R_0, and Z_0 and the segment of points used extends after each iteration; usually, after two iterations the whole profile is fitted, and two more iterations are enough to get full accuracy. The use of a subset of the experimental points during first iterations speeds up the algorithm and makes it more robust. Performance of this procedure is reported in Sec. IX A. The numerical error introduced by the procedure is quite negligible; the speed is more than 1 order of magnitude greater than reported by other authors,[6] after having accounted for the different computer speed.

VII. CALIBRATION PROCEDURE

Calibration against known values of interfacial tension should not be required with the ADSA method. Drop shape has always been considered to be the ''absolute'' method for providing the reference data for other relative techniques (see, e.g., Refs. 2 and 3, two works that have been considered for many years ''the standard'').

All physical constants that appear in Eq. (3), namely g, D_1, and D_2 can be known with a sufficient level of accuracy; β and R_0 are the results of measurements. The last missing element is the scale factor that converts pixels to metrical units. This factor has to be measured directly through a calibration procedure. In this respect sessile drop offers an advantage over the pendant one, as it is possible to put a small accurately spherical ball on the orifice that will support the liquid drop and the ball profile will be seen exactly at the same position as the drop profile. The ratio of the true diameter of the ball over its measure in pixels as seen by the video camera yields the required calibration factor. For calibration we have used a small rubin ball with 6 ± 0.001 mm diameter and a sphericity of ± 0.001 mm (Comadur SA, Le Locle, CH). It should be noted that even an error of a fraction of a millimeter in the position of the ball leads to an error in the calibration factor sensibly greater than the error on the reference ball itself.

There are several minor sources of error that have always been neglected by previous authors and can affect results to a significant level in high accuracy measurements. Routinely we take care of the following:

(i) densities D_1 and D_2 depend on temperature;
(ii) density of the solution in which the liquid drop is immersed varies with solution composition; and
(iii) index of refraction of solution depends upon both the solution composition and temperature.

Accounting for the first and second effect is straightforward: densities for liquids we use are tabulated and values at actual temperature and solution composition are used during computations.

Correction for the third effect is a bit more tricky and requires a knowledge of the variation of scale factor $S(l)$ as a function of the drop distance l from the video camera optics. This quantity has to be determined only once and remains valid until the cell geometry is changed. To get this factor the measuring cell with the calibration ball inside is moved by a micrometric movement a few millimeters back and forth, changing the distance from the optics, while registering for each position the ball image size (in pixels). For a small displacement, the scale factor changes linearly with displacement. From elementary optics, the apparent position of an object immersed in a liquid with refraction index n_l, as seen from air through a plane window, is $L' = L \cdot n_a / n_l$,

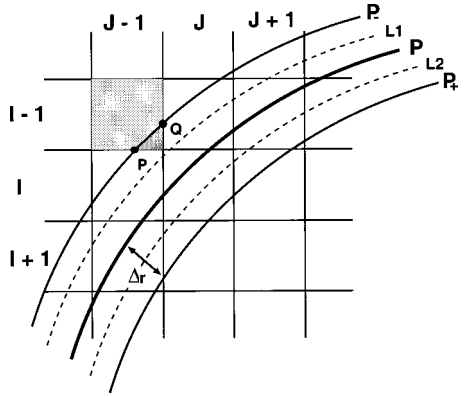

FIG. 5. Calculation of pixel illumination: a transition region from light to dark cut into two slices is shown. Profile P_-, the external border of the transition region, cuts pixel $I-1$, $J-1$ from P to Q. The outer part of the pixel surface receives full background light intensity; the inner part receives light with intensity L_1, the average value for the slice.

where L is the geometrical path of light in the liquid and n_a is the air refraction index. Then the apparent position of the drop (or the calibration ball) changes with refraction index as

$$\Delta L = L \cdot n_a \left(\frac{1}{n_l + \Delta n_l} - \frac{1}{n_l} \right) \simeq -L \frac{n_a}{n_l^2} \Delta n_l \tag{12}$$

and the scale factor changes as

$$\Delta S = -\frac{\partial S}{\partial l} \cdot L \cdot \frac{n_a}{n_l^2} \cdot \Delta n_l . \tag{13}$$

The effect is small but not quite negligible; when working with concentrated electrolytical solutions it can amount to 0.1%. We use Eq. (13) to account for it.

VIII. THE SIMULATION PROCEDURE

We have implemented a software package that simulates the full process of sessile (or pendant) drop measurements. The package includes the procedures described above for the profile extraction and fit, as well as further procedures for the synthetic generation of a pseudoexperimental frame containing a drop image. The characteristics of the drop (β and R_0) can be given or chosen at random; the drop profile is computed by numerical integration of Eq. (4), and scaled and translated as required; thereafter, the illumination value of every pixel in the frame is computed. Alternatively, an integral quantity of the drop—surface or volume—can be specified together with γ (and the supporting border radius) and β and R_0 are then obtained by an inverse algorithm. The light intensity profile across the transition region, from light to dark, can be selected among some predefined functions or given in a data file in a tabulated form. To calculate pixel illumination, the transition region is cut in many narrow slices by repeating many times the drop profile, both inward and outward, every time displacing each point normally to the profile by a fixed amount Δr (Fig. 5). An average light intensity is attributed to each one of the resulting slices equal to the value in the middle of the slice, as given by the selected function. Then the displaced profiles are followed one at a time, determining in sequence the pixels that are traveled and for each one of them the entry and exit point. The profile inside the pixel is approximated as a segment, the area of the polygonals external and internal to the profile are computed and their contribution to pixel illumination is added into an array representing the frame; pixels are considered as squares that cover the frame surface completely. Once all displaced profiles have been processed, the outer region is filled with the light background value and the inner region with the dark value. These two values also define the gray scale of the intensity profile, which is the number of gray levels to be used. When the synthetic frame has been completed, it is analyzed to recover the profile and computed back to β and R_0. Results are then compared with the starting values.

Apart from the obvious problem of making sure that the implemented code for frame processing is error free, the simulation package is very useful to evaluate the effect of several sources of error on the results of ADSA measurements and to compare different algorithms. To this purpose, during each step of the synthetic frame generation, several kinds of error or distortion can be introduced and their influence on the final result can be appreciated. Currently, the package offers the possibility of:

(i) selecting the frame size, in pixel;
(ii) introducing an asymmetry in the X and Z scale factors to simulate a possible asymmetry in the optics or in the pitch of pixel rows or columns in the sensor;
(iii) tilting the profile a small angle (to simulate a misalignment between the Z axis of the CCD sensor and the local vertical);
(iv) adding random displacements to the synthetic profile coordinates;
(v) shifting the dark and light levels and changing the gray level resolution;

TABLE I. Performance of the fit routine for several integration step sizes; the pseudoexperimental profile is always generated with step 0.0018.

Step	$\Delta\gamma/\gamma$	$\langle \Delta p^2 \rangle^{1/2}$/pixel	Time/ms
0.0018	$<10^{-6}$	13×10^{-6}	31
0.003	$<10^{-6}$	13×10^{-6}	24
0.005	$<10^{-6}$	14×10^{-6}	19
0.007	$<10^{-6}$	22×10^{-6}	16
0.010	$<10^{-6}$	62×10^{-6}	15

TABLE II. Performance of the fit routine forcing an error ΔX_0 on the estimate of X_0.

ΔX_0/pixel	$\Delta\gamma/\gamma$	ΔR_0/pixel	$\langle \Delta p^2 \rangle^{1/2}$/pixel
0.05	$<10^{-6}$	1×10^{-4}	33×10^{-3}
0.1	2×10^{-6}	3×10^{-4}	66×10^{-3}
0.2	7×10^{-6}	14×10^{-4}	132×10^{-3}

TABLE III. Effect of a tilt of the image sensor on the value of γ.

θ/mrad	$\Delta\gamma/\gamma$	$\langle \Delta p^2 \rangle^{1/2}$/pixel
0.0	1.9×10^{-5}	3×10^{-3}
0.5	1.3×10^{-5}	33×10^{-3}
1.0	1.3×10^{-5}	66×10^{-3}
2.0	1.9×10^{-5}	132×10^{-3}

TABLE IV. Performance of the profile extraction algorithms with noiseless data: intrinsic accuracy and profile extraction time.

Method	$\Delta\gamma/\gamma$	$\langle\Delta p^2\rangle^{1/2}$/pixel	Time/ms
avg	2.1×10^{-5}	$3.\times10^{-3}$	7
h2	1.1×10^{-5}	3×10^{-3}	10
h3	2.4×10^{-5}	$<\ 8\times10^{-3}$	11
p3	1.0×10^{-4}	10×10^{-3}	12

(vi) blurring the image adding random noise to every pixel in the frame (either additive or multiplicative noise or both);
(vii) blurring the image with noise that affects random clusters of pixels to simulate the effect of dust spots; and
(viii) blurring the image adding the ''smear effect'' created by the frame shifting in a CCD device.

All effects can be introduced in a predefined amount or at random. During frame analysis, operation is timed to assess relative efficiency of different algorithms.

The consistency of results obtained when no effect is introduced during the frame generation makes us confident that the code is error free. The profile integration routine cannot be validated this way, as it is a piece of code common to both frame generation and analysis, hence a systematic error in this part of the code might pass undetected. This routine has been tested comparing its results with those obtained with two other completely independent procedures: the routine described in Ref. 20, which is based on an algorithm other than Runge–Kutta integration, and integration of Eq. (4) as obtained with the package MATHEMATICA (Wolfram Research, Inc., Champaign, IL). In both cases differences among the computed profiles were at the numerical rounding level.

IX. RESULTS

Algorithms have been tested under the following conditions, unless otherwise stated:

(i) frame size: 1024×1024 pixels;
(ii) gray levels: 4096 with light at 90% and dark at 10% of the scale;
(iii) transition region profile: the ''erf'' error function, scaled 3:1 on the X axis to get a transition region $\simeq5$ pixels wide;
(iv) number of slices in the transition region: 100;
(v) γ range: $45-100\times10^3$ (γ is given as R_0^2/β, with R_0 in pixels);
(vi) drop surface: 1.1×10^6 pixel^2;
(vii) integration step for the pseudoexperimental profile: 0.0018 in adimensional coordinates, as defined in Eq. (9); this yields roughly the same number of points as obtained from a true experimental frame;
(viii) integration step during the fit: 0.005; and
(ix) execution times obtained on a Pentium III 450 MHz computer running a Linux Red Hat 6.1 operating system.

TABLE V. Performance of the profile extraction algorithms with noise level 0.5%.

Method	$\Delta\gamma/\gamma$	$\langle\Delta p^2\rangle^{1/2}$/pixel	$\langle\Delta X_0^2\rangle^{1/2}$/pixel
avg	1.3×10^{-4}	42×10^{-3}	12×10^{-3}
h2	5.4×10^{-5}	19×10^{-3}	9×10^{-3}
h3	5.7×10^{-5}	19×10^{-3}	9×10^{-3}
p3	3.1×10^{-4}	120×10^{-3}	23×10^{-3}

TABLE VI. Performance of the profile extraction algorithms with noise level 1%.

Method	$\Delta\gamma/\gamma$	$\langle\Delta p^2\rangle^{1/2}$/pixel	$\langle\Delta X_0^2\rangle^{1/2}$/pixel
avg	2.9×10^{-4}	81×10^{-3}	20×10^{-3}
h2	1.0×10^{-4}	37×10^{-3}	12×10^{-3}
h3	1.0×10^{-4}	36×10^{-3}	13×10^{-3}
p3	7.1×10^{-4}	237×10^{-3}	35×10^{-3}

For each test the evaluated error is the relative difference $\Delta\gamma/\gamma$ between the value of γ used in the synthetic frame generation and the value obtained from frame analysis. Besides, the rms value $\langle\Delta p^2\rangle^{1/2}$ of differences among the extracted profile points and the profile obtained from the fit are reported.

A. Errors from the fit routine

The pseudoexperimental profile has been given to the fit routine, without passing through the frame generation and profile extraction procedure. Computations have been repeated for different integration steps during the fit (see Table I).

In the first case the integration step is the same as used for profile generation, hence pseudoexperimental and fitted profiles coincide; accuracy remains very good even increasing the integration step.

B. Effect of X_0 error on fit accuracy

The test in Sec. IX A has been repeated (with step 0.005) forcing an error ΔX_0 into the estimate of X_0, before completing the fit over Z_0, R_0, β as usual (see Table II).

C. Effect of tilt angle

A tilt is simulated between the axis of symmetry of the drop (which is considered exactly aligned to the true local vertical) and the Z axis of the sensor (see Table III).
In this simulation the transition region was reduced to an abrupt step from light to dark.

In Tables II and III, despite the fitted and the experimental profile diverging rapidly as tilt angle or X_0 offset increases, the error on $\Delta\gamma/\gamma$ remains quite small. This is due to the intrinsic symmetry of the system; it is the exploitation

TABLE VII. Performance of the profile extraction algorithms with noise level 2%.

Method	$\Delta\gamma/\gamma$	$\langle\Delta p^2\rangle^{1/2}$/pixel	$\langle\Delta X_0^2\rangle^{1/2}$/pixel
avg	4.3×10^{-4}	162×10^{-3}	29×10^{-3}
h2	2.1×10^{-4}	74×10^{-3}	19×10^{-3}
h3	1.9×10^{-4}	68×10^{-3}	19×10^{-3}
p3	32×10^{-4}	440×10^{-3}	58×10^{-3}

TABLE VIII. Errors due to the smearing effect produced by the frame shift in the CCD video camera.

sm	$\Delta\gamma/\gamma$	$\langle\Delta p^2\rangle^{1/2}$/pixel
10×10^{-6}	2.6×10^{-5}	3.5×10^{-3}
20×10^{-6}	4.2×10^{-5}	3.6×10^{-3}
30×10^{-6}	6.3×10^{-5}	3.7×10^{-3}
50×10^{-6}	1.1×10^{-4}	4.1×10^{-3}
100×10^{-6}	2.3×10^{-4}	4.7×10^{-3}
150×10^{-6}	3.4×10^{-4}	7.8×10^{-3}

of this property that allows the use of a simplified and faster fit algorithm that performs minimization over only three adjustable parameters.

D. Comparison among several profile extraction algorithms

Four algorithms for profile extraction have been tested under different noise conditions:

(i) avg: center of mass algorithm—edge position is given by center of mass of differences of adjacent pixels;
(ii) h2: ''halfway method'' as in Ref. 16—edge position is obtained by linear interpolation between closest values above and below fraction 0.5;
(iii) h3: same as h2, but three points and linear least squares fit are used; and
(iv) p3: maximum gradient method—edge position is obtained by parabolic interpolation of three differences between adjacent pixels centered around the highest value.

Noise has been added to each pixel in the frame as a random value with Gaussian distribution and standard deviation proportional to the pixel intensity.

Tables IV–VII are tests of the overall accuracy of the algorithms for generating the pseudoexperimental frame and extracting back the drop profile. Reported time refers to profile extraction alone; overall times are reported in Sec. IX F.

The maximum gradient method, in the simple parabolic form we tested, is not suitable to be used with a high noise level.

E. Effect of image smearing as produced by the frame shift in CCD devices

Smear sm is measured as the ratio between the time required to shift the frame one line during the frame-transfer period over the integration time. This effect has always been ignored by previous authors; yet it can become a heavy source of error when using a lower grade CCD sensor. In the MX12P-8443 video camera, as we currently use it, $\mathrm{sm}=33\times10^{-6}$ (see Table VIII).

The above results have been obtained simulating an upward frame shift; the test has been repeated reversing the shift direction (i.e., ''using'' the video camera upside down) obtaining similar results.

TABLE IX. Cumulative effect of all source of errors and overall time requirement.

Method	$\Delta\gamma/\gamma$	$\langle\Delta p^2\rangle^{1/2}$/pixel	Time/ms
avg	1.8×10^{-4}	82×10^{-3}	32
h2	1.1×10^{-4}	56×10^{-3}	36
h3	1.1×10^{-4}	51×10^{-3}	37
p3	6.3×10^{-4}	244×10^{-3}	38

F. Cumulative error

In this test all sources of error have been combined to reflect our experimental conditions:

(i) tilt angle $\theta=0\pm0.5$ mrad;
(ii) noise $=\pm1\%$; and
(iii) smear $=33\times10^{-6}$

obtaining the following overall performance (Table IX).

It should be noted that the overall error is well below measurement reproducibility due to other experimental conditions as, e.g., errors due to the chemical system purity, stability, and reproducibility. Hence it is not a correct procedure to compare algorithm performances through true experimental measurements.

ACKNOWLEDGMENTS

This work is dedicated to Professor Silvano Bordi, who originated and encouraged it for many years. Financial support from I.N.F.M. (Istituto Nazionale per la Fisica della Materia) and MURST on ''60%'' and ''Cofinanziamento 40%'' funds is acknowledged.

[1] F. Bashforth and J. C. Adams, *An Attempt to Test the Theories of Capillary Action* (Cambridge University Press, Cambridge, 1883).
[2] C. A. Smolders and E. M. Duyvis, Recl. Trav. Chim. Pays-Bas. **80**, 635 (1961).
[3] H. Vos and J. M. Los, J. Colloid Interface Sci. **74**, 360 (1980).
[4] B. Song and J. Springer, J. Colloid Interface Sci. **184**, 64 (1996).
[5] P. Chen, O. I. del Rio, and A. W. Neumann, in *Axisymmetric Drop Shape Analysis* edited by A. Bazskin and W. Nord, Physical Chemistry of Biological Interfaces (Marcel Dekker, New York, 2000), p. 523.
[6] S. Lahooti, O. I. del Rio, A. W. Neumann and P. Cheng, in *Axisymmetric Drop Shape Analysis (ADSA)*, edited by A. W. Neumann and J. K. Spelt, Applied Surface Thermodynamics (Marcel Dekker, New York, 1996), p. 441.
[7] A. J. P. Theuwissen, *Solid State Imaging with Charge-Coupled Devices* (Kluwer, Dordrecht, 1995).
[8] L. Busoni, M. Carlà, L. Lanzi, L. Dei, and M. Olivotto, Phys. Chem. Chem. Phys. **2**, 5698 (2000).
[9] S. Bordi, M. Carlà, and R. Cecchini, Electrochim. Acta **34**, 1673 (1989).
[10] The full package is available freely from authors under the terms of the GPL software license, i.e., complete with the source code and freely usable and redistributable. For information about General Public License (GPL) see www.gnu.org.
[11] M. Carlà, R. Cecchini, and S. Bordi, Rev. Sci. Instrum. **62**, 1088 (1991).
[12] M. Carlà, Meas. Sci. Technol. **4**, 473 (1993).
[13] P. Seitz, Opt. Eng. **27**, 535 (1988).
[14] N. R. Pallas and Y. Harrison, Colloids Surface **43**, 169 (1990).
[15] F. K. Hansen, J. Colloid Interface Sci. **160**, 209 (1993).
[16] B. Song and J. Springer, J. Colloid Interface Sci. **184**, 77 (1996).
[17] F. K. Hansen and G. Rodsrud, J. Colloid Interface Sci. **141**, 19 (1991).
[18] T. Kakiuchi, M. Nakanishi, and M. Senda, Bull. Chem. Soc. Jpn. **61**, 1845 (1988).
[19] W. H. Press *et al.*, *Numerical Recipes: The Art of Scientific Computing* (Cambridge University Press, Cambridge, 1986).
[20] J. Butler and B. Bloom, Surf. Sci. **4**, 1 (1966).